Available online at www.sciencedirect.com
ScienceDirect
Journal of Power Sources 160 (2006) 1314–1319
JOURNAL OF POWER SOURCES
www.elsevier.com/locate/jpowsour

Behavior of the monophosphate tungsten bronzes $(PO_2)_4(WO_3)_{2m}$ ($m = 4$ and 6) in electrochemical lithium insertion

F.E. Longoria Rodríguez, A. Martínez-de la Cruz *, E. López Cuéllar

División de Estudios de Posgrado, Facultad de Ingeniería Mecánica y Eléctrica, Universidad Autónoma de Nuevo León, Pedro de Alba s/n, Ciudad Universitaria, C.P. 66451, San Nicolás de los Garza, NL, Mexico

Received 24 January 2006; received in revised form 8 February 2006; accepted 9 February 2006
Available online 17 April 2006

Abstract

The electrochemical lithium insertion process has been studied in the family of monophosphate tungsten bronzes $(PO_2)_4(WO_3)_{2m}$, where $m = 4$ and 6. Structural changes in the pristine oxides were followed as lithium insertion proceeded. Through potentiostatic intermittent technique, the different processes which take place in the cathode during the discharge of the cell were analysed. The nature of the bronzes $Li_x(PO_2)_4(WO_3)_{2m}$ formed was determined by in situ X-ray diffraction experiments. These results have allowed establishment of a correlation with the reversible/irreversible processes detected during the electrochemical lithium insertion. Measurements of resistivity showed that upon lithium insertion, the metallic pristine oxides become insulating.

Keywords: Lithium insertion; Batteries; Tungsten bronzes

1. Introduction

The extended family of bronzes known as phosphate tungsten bronzes has received special attention due to their interesting potential to develop electronic displays [1–3]. In general, these bronzes are formed when a WO_6 unit is replaced by monophosphate (PO_4) or diphosphate (P_2O_7) groups in the ReO_3-type structure of the WO_3. Under this crystallographic base, three structural frameworks can be built to form: (a) the monophosphate tungsten bronzes with pentagonal tunnels ($MPTB_p$) with general formula $(PO_2)_4(WO_3)_{2m}$, (b) the monophosphate tungsten bronzes with hexagonal tunn*els* ($MPTB_h$) described by $A_x(PO_2)_4(WO_3)_{2m}$, and (c) the diphosphate tungsten bronzes with hexagonal tunnels ($DPTB_h$) and general formula $A_x(P_2O_4)_2(WO_3)_{2m}$ [4]. In order to stabilize the crystalline structure by the existence of large hexagonal tunnels in the cases (b) and (c), an atom A (typically A = Na, K, Cs) with appropriate ionic radii should be inserted in the hexagonal holes. In contrast, the monophosphate tungsten bronzes with pentagonal tunnels ($MPTB_p$) provide empty pentagonal tunnels that are available to accommodate a chemical species through an insertion reaction.

Different features of these materials, i.e. (a) its framework based in the perovskite type structure produces an open structure suitable for lithium insertion reactions, and (b) the high oxidation state of the transition metal that forms the framework, suggest a large amount of lithium could be inserted.

Recently in our group we have started a systematic study of the ability of these bronzes to insert small ions like lithium [5–7]. In the present work, an electrochemical lithium insertion study into two members of the family of $MPTB_p$, $(PO_2)_4(WO_3)_{2m}$ with $m = 4$ and 6 is presented. These bronzes are thermodynamically stable phases in the region with a higher content of phosphorus in the phase diagram P_2O_5–WO_3. Their structures are the product of replacement of some WO_6 octahedra units by PO_4 tetrahedra groups with the subsequent loss of oxygen to adjust the stoichiometry, see Fig. 1. The value of m is an integer related to the thickness of the ReO_3-type slabs, and for the series $(PO_2)_4(WO_3)_{2m}$ can take a value between $2 \leq m \leq 14$ [8].

2. Experimental

The phosphate tungsten bronzes, $P_4W_8O_{32}$ and $P_4W_{12}O_{44}$, were obtained in two steps. In the first instance, mixtures of

* Corresponding author. Tel.: +52 81 83 29 40 20; fax: +52 81 83 32 09 04.
E-mail address: azmartin@gama.fime.uanl.mx (A. Martínez-de la Cruz).

0378-7753/$ – see front matter © 2006 Elsevier B.V. All rights reserved.
doi:10.1016/j.jpowsour.2006.02.049

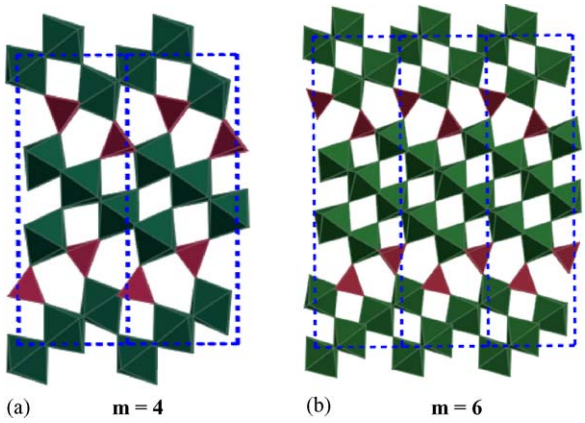

Fig. 1. Schematic representation of the crystalline structures of bronzes $(PO_2)_4(WO_3)_{2m}$. (a) $P_4W_8O_{32}$ and (b) $P_4W_{12}O_{44}$.

$(NH_4)_2HPO_4$ and WO_3 in a molar ratio 1:1.83 and 1:2.83 respectively, were heated in air at 923 K in order to decompose the ammonium phosphate. Then, a stoichiometric amount of W was added to the starting mixtures to reach the appropriate composition in each bronze. After grinding, each mixture was placed in a quartz tube that was evacuated, sealed and heated at 1273 K for 9 days and then slowly cooled to room temperature.

Structural characterization was carried out by X-ray diffraction using a Siemens D-5000 diffractometer with Cu K_α ($\lambda = 1.5418$ Å) radiation. X-ray diffraction data of pristine oxides were collected in the 2θ range of 5°–90° with a scan rate of 0.05°/2 s. Taking into account the poor crystallinity of lithiated bronzes, they were analyzed using a scan rate of 0.01°/8 s in the 2θ range of 5°–60°.

The electrochemical lithium insertion was studied by means of an electrochemical cell of the Swagelok type with metallic lithium as the negative electrode. The positive electrode was a 7 mm diameter pellet obtained by pressing 15–25 mg of a mixture containing the material active, carbon black and ethylene-propylene-diene-terpolymer (EPDT) in a 89:10:1 ratio. For the electrolyte a 1 mol dm^{-3} solution of $LiPF_6$, in a mixture of ethylene carbonate (EC) and dimethyl carbonate (DMC) 50:50, was used. Due to the high reactivity of metallic lithium, the assembly of the cells was carried out in argon filled glove box (MBraun) with a content of oxygen and water less than 1 ppm. The assembled cell was then removed and connected to a multichannel galvanostatic-potentiostatic system (MacPile II). In a typical potentiostatic experiment a voltage scanning rate of ±10 mV 0.5 h^{-1} was applied during the cell cycles between different values of voltage versus Li^+/Li^0.

The evolution of structural changes in the framework of the host as lithium insertion proceeded was followed in situ by X-ray diffraction technique. For this purpose an electrochemical cell was developed [9]. The cell was designed with a dual function: as sample holder and as electrochemical cell. Different cells were tested under open circuit voltage conditions, applying a current density of 390 μA cm^{-2} for 1.5–2.0 h and relaxing the cell for a similar time. According to the electrode mass, an increase of about 1.0, 2.0, 3.0 and 4.0 Li per formula was reached in each step. Only when the system was relaxed (variation of voltage with the time smaller than 20 mV h^{-1}) was the X-ray diffraction data recorded. This process was performed slowly due to the poor crystallinity of the lithiated phases. Typically a scan rate of 0.05° 2 s^{-1} in a 2θ range from 5° to 60° was used.

Resistivity measurements of samples of composition $Li_x(PO_2)_4(WO_3)_{2m}$ ($m = 4$ and 6) with $x \geq 0$, were made using pellets of 0.2 cm^2 area. For these experiments, pellets of $P_4W_8O_{32}$ and $P_4W_{12}O_{44}$ were heated at 1273 K for 14 days in an evacuated quartz tube in order to reduce the grain boundaries and then were cooled slowly to room temperature. These pellets were utilized to synthesize bronzes with composition $Li_xP_4W_8O_{32}$ and $Li_xP_4W_{12}O_{44}$ through electrochemical methods. Different cells were discharged up to certain predetermined compositions at a scanning voltage rate of −10 mV h^{-1}. The final composition of the samples was determined by associating the current that flowed through the external circuit with the amount of lithium inserted according with Faraday's law. The electrochemical cells were opened within a dry box, the pellets were removed, dried and then covered with a gold layer in both sides to make a good electrical contact. Resistivity measurements were made under a nitrogen atmosphere in a cell developed for this specific purpose. The electrical behavior of the samples was evaluated in an Impedance Analyzer HP4284A in a frequency range of 10 Hz–1000 kHz and a temperature range of 193–298 K.

3. Results and discussions

Fig. 2 shows the typical potential variation related to the amount of lithium inserted when two cells with a configuration: Li/electrolyte/$(PO_2)_4(WO_3)_{2m}$ (with $m = 4$ and 6, respectively), were cycled in the potential range 3.5–0.01 V versus Li^+/Li^0 under potentiostatic conditions. In the first cycle, the maximum amount of lithium inserted, approximately 52 and 72 lithium atoms per formula in each case, led to a high specific capacity of 600 Ah kg^{-1} in each bronze studied. Nevertheless, near half of specific capacity was lost after the first charge–discharge cycle due to the inability of the system to remove around 50% of lithium inserted during the charge process.

Note that these compositions exceed the theoretical values of $Li_{44}P_4W_8O_{32}$ and $Li_{68}P_4W_{12}O_{44}$ if we assume the full reduction from $W^{5.5+}$ and $W^{5.66+}$, respectively, to W metal in the hosts matrix. Such a phenomenon has been detected for several oxides included niobium phosphates [10], which are decomposed at low potentials and from which the extra capacity of the cell is associated with carbon reduction and/or formation of passivation layers from electrolyte decomposition below 1 V versus Li^+/Li^o [11].

In order to investigate details of the lithium insertion in $P_4W_8O_{32}$ and $P_4W_{12}O_{44}$, the different processes involved in the insertion electrode during the charge–discharge of the cell were analyzed. The changes in slope detected in the *E*–*x* plots of Fig. 2 can be associated directly with phase transitions. In a first interpretation, the regions where a continuous variation of the potential with composition was observed, correspond to single phases (regions labeled as I–III in Fig. 2) whereas voltage

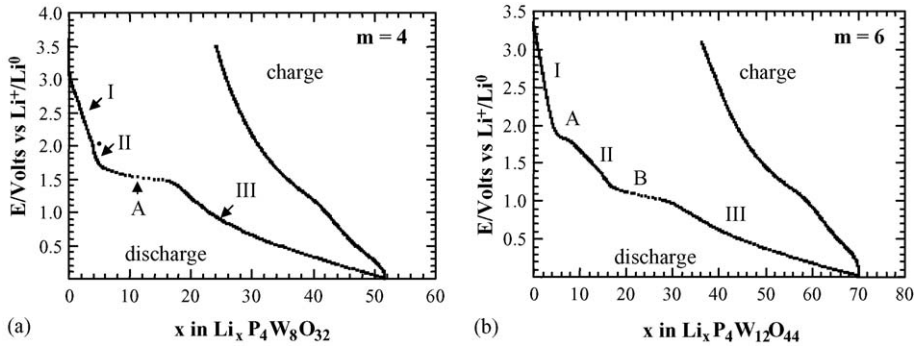

Fig. 2. Voltage–composition plots for a charge–discharge cycle of two cells with configuration Li//$(PO_2)_4(WO_3)_{2m}$ under potentiostatic conditions.

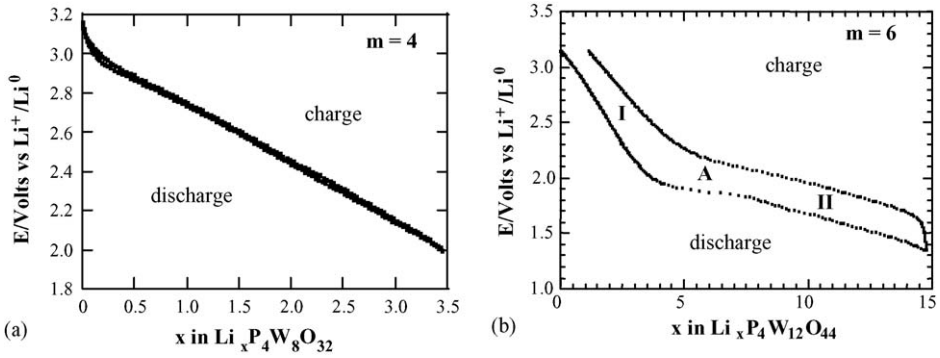

Fig. 3. Voltage–composition plots for a charge–discharge cycle of two cells with configuration Li//$(PO_2)_4(WO_3)_{2m}$ when it were cycled until (a) 2.0 V for $P_4W_8O_{32}$ and (b) 1.35 V for $P_4W_{12}O_{44}$.

plateaus (labeled as A and B) can be assigned with a biphase region, where a first order transition takes place. Although all these features are clearly observed during the discharge processes when the direction of scan voltage is inverted (charge processes), some of these features disappear showing the irreversible nature of at least one process during insertion.

To know the nature of each transition, cell cycles of the Li/electrolyte/$(PO_2)_4(WO_3)_{2m}$ (with $m = 4$ and 6) were carried out under the same conditions already mentioned. The cells were discharged to the minimum voltage limit just above where each biphase region was found. Fig. 3 shows a charge–discharge cycle for each bronze, (a) $P_4W_8O_{32}$ and (b) $P_4W_{12}O_{44}$, to a limit potential where the lithium insertion process was reversible. As can be observed in Fig. 3a, the origin of irreversibility in the system Li//$P_4W_8O_{32}$ is associated with the process previously labeled as A (II → III, 1.5 V versus Li^+/Li^o). On the other hand Fig. 3b shows that for $P_4W_{12}O_{44}$ an irreversible lithium insertion reaction is associated with the process labeled as B (II → III, 1.0 V versus Li^+/Li^o).

To confirm our first interpretation of the *E*–*x* plots, potentiostatic experiments were analyzed to observe the current relaxation with time at each voltage step, as can be seen in Fig. 4 for the lithium insertion process into $P_4W_8O_{32}$. For potential values where voltage varies continuously with the composition in Fig. 4a, i.e. I and II regions, the behavior of current with time is homogeneous and decays to zero in each potential step. This situation indicates that the system is crossing a solid solution region and lithium insertion is governed by the ion diffusion process. Note that regions I and II are separated by a zone where the capacity of the cell decays near to zero (labeled as •). Taking into account that such a process takes place between two single phases, it can be associated with a continuous phase transition

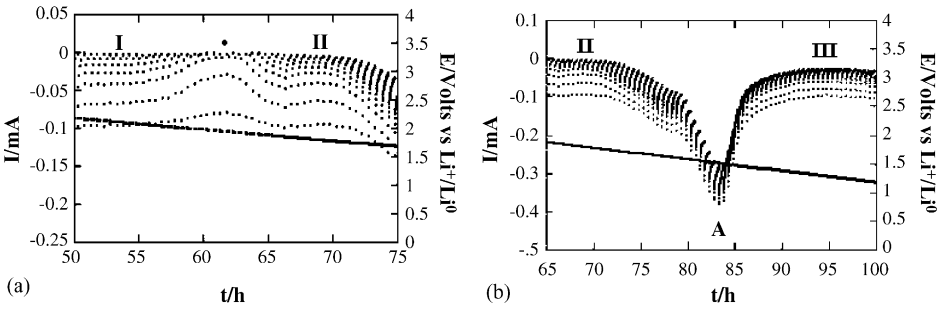

Fig. 4. Chronoamperogram obtained by discharging a cell Li//$P_4W_8O_{32}$ at a scan rate of −10 mV/0.5 h.

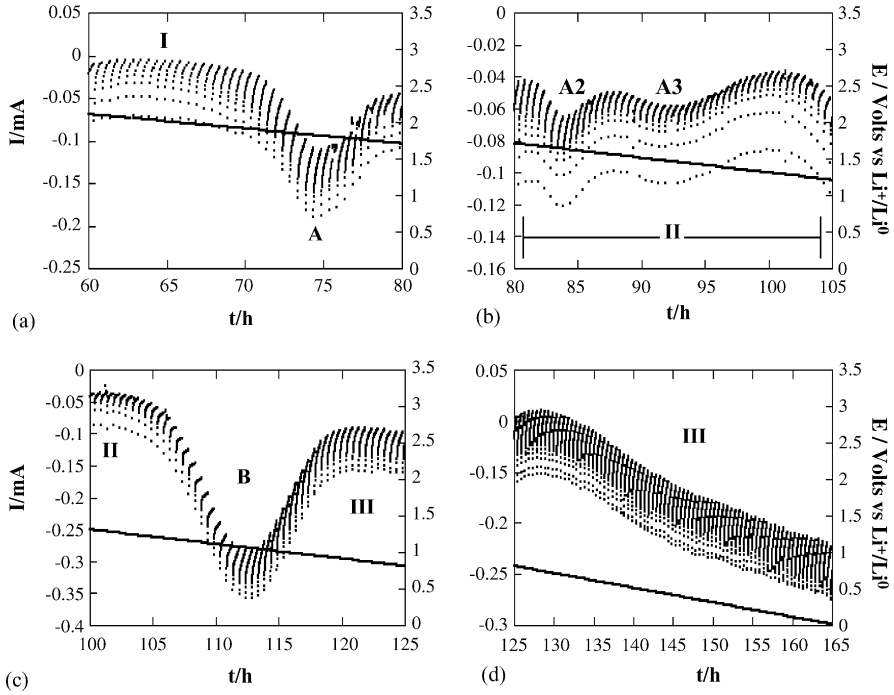

Fig. 5. Chronoamperogram obtained by discharging a cell Li//$P_4W_{12}O_{44}$ at a scan rate of −10 mV/0.5 h.

[12]. On the other hand, in Fig. 4b for potential values around the peak labeled as *A*, the current increases reaching a maximum value at 1.5 V versus Li^+/Li^o. In this case, the behavior of current with time is far from a $t^{-1/2}$ law, which corresponds with a first order transition (heterogeneous behavior in the *I–t* curves for each potential step). Similar conclusions were obtained when *I*(*t*) curves for lithium insertion in $P_4W_{12}O_{44}$ were analysed, as can be appreciated in the Fig. 5. Nevertheless, in this case, a detailed analysis of the *I–t* curves showed that the region labelled as II involves two processes, labelled as A2 and A3 in Fig. 5b.

Some similar features have been observed in the course of electrochemical lithium insertion in $P_4W_8O_{32}$ and $P_4W_{12}O_{44}$. In the first instance, the first four lithium atoms are inserted through a reversible mechanism that involves the formation of a single phase. In Fig. 1, we can observe four pentagonal and six quadrangular tunnels per unit cell in $P_4W_8O_{32}$, and four pentagonal and 10 quadrangular tunnels in $P_4W_{12}O_{44}$. So, a possible explanation for the similar behavior between both bronzes is that the first four lithium atoms are inserted through the pentagonal tunnels. After this step in $P_4W_8O_{32}$ an irreversible process takes place and is observed as a large plateau (labeled as A), around 1.5 V versus Li^+/Li^0. An equivalent process is observed in $P_4W_{12}O_{44}$ at 1.3 V versus Li^+/Li^0 (B), and appeared after a second region of continuous variation of potential with respect composition (II). In this region, absent in $P_4W_8O_{32}$, up to 12 lithium atoms per formula were inserted, i.e. One lithium atom per W in $P_4W_{12}O_{44}$. This agreement between the amount of lithium inserted and the amount of tungsten per unit formula was also observed for each bronze $Li_x(PO_2)_4(WO_3)_{2m}$ with $m \geq 6$ [13]. Note that for monophosphate tungsten bronzes with $m \geq 6$ structural features of ReO_3-type structure are present, i.e. quadrangular holes surrounded by four WO_6-octahedra, where according with previous studies in related oxides near of one lithium atom can be inserted per W atom [14].

In situ X-ray diffraction experiments during the discharge of the electrochemical cells were carried out in order to characterize the detected phases $Li_xP_4W_8O_{32}$ and $Li_xP_4W_{12}O_{44}$. Fig. 6 shows the X-ray diffraction patterns of $Li_xP_4W_8O_{32}$ where $0 \leq x \leq 14$. For small quantities of lithium inserted, i.e. $0 \leq x \leq 4$, diffraction pattern of the pristine oxide is maintained with a slight shift of their diffraction lines. For high lithium contents, i.e. $x \geq 4$, diffraction lines fades until disappear for lithium composition of $x = 14$ and then the material active becomes amorphous. We are now able to correlate electrochemical data with structural changes in the host matrix of bronze. We can

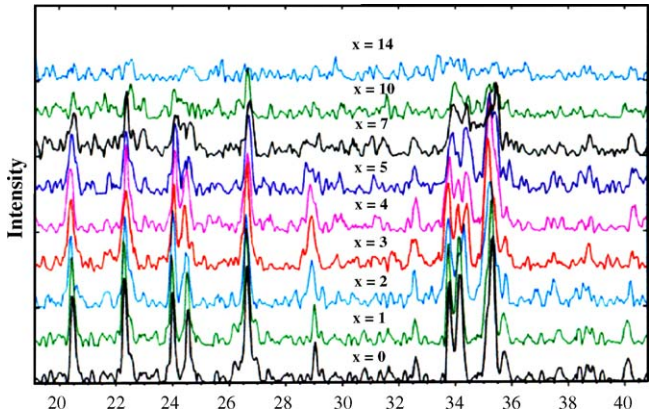

Fig. 6. X-ray diffraction patterns of $Li_xP_4W_8O_{32}$ obtained during the electrochemical lithium insertion.

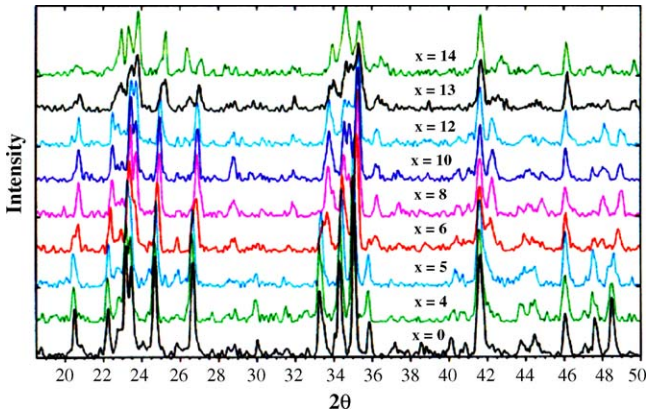

Fig. 7. X-ray diffraction patterns of $Li_xP_4W_{12}O_{44}$ obtained during the electrochemical lithium insertion.

establish that the irreversible nature of process labeled as *A*, which appears for $x > 4$ in $Li_xP_4W_8O_{32}$, is associated with an irreversible structural transformation of the parent oxide.

Fig. 7 shows the X-ray diffraction patterns of samples $Li_xP_4W_{12}O_{44}$ where $0 \leq x \leq 14$. At low values of lithium concentration, see, e.g. $x = 4$, the orthorhombic $P_4W_{12}O_{44}$ matrix is practically maintained without loss of crystallinity. Note that this sample corresponds to a region where a continuous variation of the potential with composition is observed (single phase assigned to region I in Fig. 2b). As insertion proceeds, a second abrupt change of potential is detected for a slight variation in composition (region II in Fig. 2b). In this case a study by X-ray diffraction showed that, for a sample with composition within this region (see, e.g. $x = 8$ in Fig. 7), a new phase, with a variable composition and monoclinic symmetry, is formed (monoclinic a). As was proposed from the electrochemical results, between these solid solution regions a two-phase domain should exist (region A in Fig. 2b). Note that in the Fig. 7 the samples corresponding to this region, $x = 5$ and 6, are formed by a mixture of orthorhombic and monoclinic phases.

A similar situation is detected when lithium insertion proceeds at a higher ion concentration. Thus, for a sample with composition in the region between A2 and A3 in Fig. 5b (see, e.g., $x = 12$, in Fig. 7) the X-ray diffraction diagram shows the existence of a new phase of variable composition and monoclinic symmetry (monoclinic b). A similar agreement between electrochemical and structural characterization data was observed for $x = 14$, in the region between A3 and B (monoclinic c). For $Li_xP_4W_{12}O_{44}$ with $15 \leq x \leq 30$ (region B) the diffraction lines fade and disappear for lithium a composition of $x = 22$, then the active material becomes amorphous. In this case, the irreversible nature of the process labeled as B, is associated with an irreversible structural transformation of the parent oxide. Finally, in the last region of single phase labeled as III in Fig. 2b, the active material was amorphous for all compositions studied.

Table 1
Relation of the phases $Li_xP_4W_8O_{32}$ detected by electrochemical study and characterized by X-ray diffraction technique

x in $Li_xP_4W_8O_{32}$	a (Å)	b (Å)	c (Å)	R-factor
0	5.283(6)	6.569(0)	17.355(3)	3.09
1	5.283(8)	6.568(9)	17.371(8)	3.23
2	5.283(1)	6.568(7)	17.400(3)	3.65
3	5.283(4)	6.569(2)	17.419(0)	2.89
4	5.283(6)	6.568(7)	17.453(8)	3.99

Taking into account the experimental conditions for the collection of X-ray data and the nature of the lithium insertion compounds, is very difficult to obtain data that can be processed by refinement analyses. Although it was possible to assign all diffraction lines to a specific crystallographic cell with the X-ray in situ data, is very difficult to estimate with precision the cell parameters. In order to reach this goal, some selected bronzes $Li_xP_4W_8O_{32}$ and $Li_xP_4W_{12}O_{44}$ were prepared by electrochemical methods in a Swagelok type cell for subsequent study. Tables 1 and 2 shows the refinement data of the lithiated phases that represents each region of the *E*–*x* diagrams previously discussed.

The behavior of conductivity with respect to temperature (174–298 K) of the bronzes $Li_xP_4W_8O_{32}$ and $Li_xP_4W_{12}O_{44}$ is shown in Figs. 8 and 9, respectively. For all samples analyzed in the single-phase region $Li_xP_4W_8O_{32}$ (labeled as I in Fig. 2a), the conductivity increases as the temperature decreases which corresponds with an electronic conductor. As lithium insertion proceeds, a slightly increase in the value of the Ea of the process was observed, having values from 0.14 eV for the parent oxide to 0.69 eV for the sample with a higher amount of lithium within the single phase, i.e. $Li_4P_4W_8O_{32}$. Samples with $x = 5$ and 6 are also included, although both belong to the biphase region A.

A similar behavior was observed in the relationship of conductivity/temperature for the samples with composition $Li_xP_4W_{12}O_{44}$, see Fig. 9. In this case, the values of Ea were from 0.24 eV for the parent oxide to 0.88 eV for $Li_{16}P_4W_{12}O_{44}$. Measurements of resistivity at 298 K show that upon lithium

Table 2
Relation of the phases $Li_xP_4W_{12}O_{44}$ detected by electrochemical study and characterized by X-ray diffraction technique

x in $Li_xP_4W_{12}O_{44}$	Region	Crystal system	Space group	a (Å)	b (Å)	c (Å)	β (°)	R-factor
0	I	Orthorhombic	$P2_12_12_1$	5.292(9)	6.559(0)	23.545(7)	90	3.02
1	I	Orthorhombic	$P2_12_12_1$	5.290(1)	6.557(8)	23.557(0)	90	4.60
2	I	Orthorhombic	$P2_12_12_1$	5.288(7)	6.558(5)	23.564(1)	90	3.75
3	I	Orthorhombic	$P2_12_12_1$	5.288(8)	6.557(8)	23.575(0)	90	2.91
4	I	Orthorhombic	$P2_12_12_1$	5.288(9)	6.560(0)	23.584(2)	90	2.99
8	II	Monoclinic a	–	17.514(0)	9.677(2)	18.702(9)	92.8	5.04
12	II	Monoclinic b	–	17.308(0)	4.813(6)	18.079(6)	98.3	6.42
14	II	Monoclinic c	–	21.251(8)	3.789(4)	23.311(5)	104.1	5.73

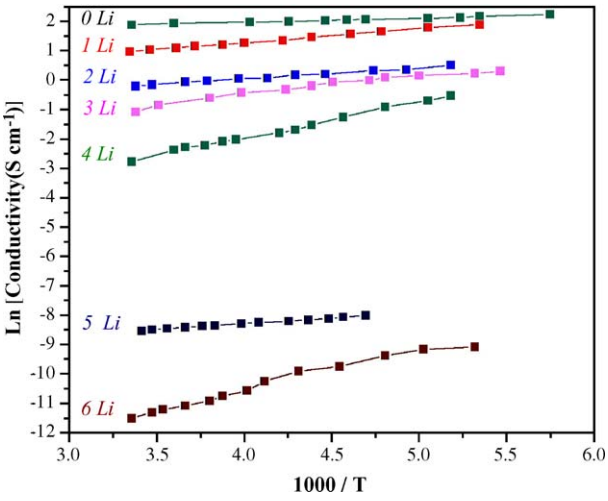

Fig. 8. Variation of the ln[conductivity (S/cm)] as a function of the temperature and amount of lithium inserted in the bronze $Li_xP_4W_8O_{32}$.

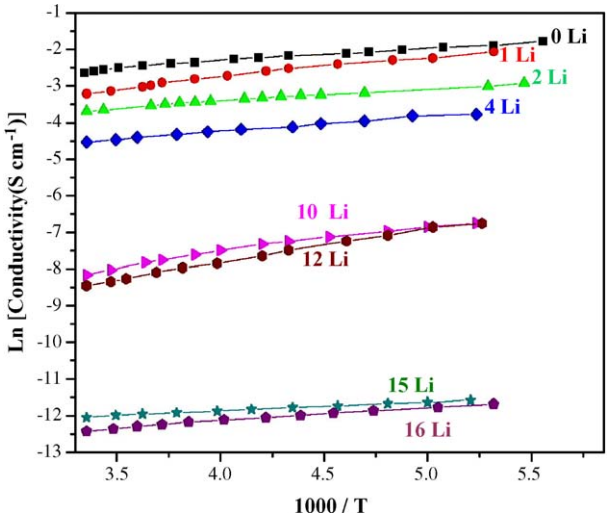

Fig. 9. Variation of the ln[conductivity (S/cm)] as a function of the temperature and amount of lithium inserted in the bronze $Li_xP_4W_{12}O_{44}$.

insertion the metallic pristine oxide becomes insulating. In the course of lithium insertion, three types of behavior were detected according to the amount of lithium inserted: conductor in phase I, semiconductor in phase II, and an insulator in phase III. This behavior has been already explained for similar phosphate tungsten bronzes [15]. Taking into account that $P_4W_8O_{32}$ and $P_4W_{12}O_{44}$ are metallic conductors, lithium insertion presumably results in the filling of the W–O–W hybridized π^* conduction band with the subsequently change from metal to insulating properties.

4. Conclusions

Electrochemical lithium insertion in $P_4W_8O_{32}$ and $P_4W_{12}O_{44}$ proceeded through a mechanism that involved the existence of single-and two-phase regions. Different compositions in the whole range $Li_xP_4W_8O_{32}$ and $Li_xP_4W_{12}O_{44}$ have been studied by X-ray diffraction, and the corresponding results perfectly correlate with the electrochemical characterization. Measurements of resistivity showed that upon lithium insertion the metallic pristine oxides become insulating. In the course of lithium insertion three types of behavior were detected according with the phases formed: metallic, semiconductor, and insulator.

Acknowledgements

We wish to thank to CONACYT for supporting the project 43800 and the Universidad Autónoma de Nuevo León (UANL) for its invaluable support through the project PAICYT-2004. We also thanks to MSc Jorge Ibarra Rodriguez for his kind help in the conductivity measurements.

References

[1] P. Roussel, O. Pérez, Ph. Labbé, Acta Cryst. B57 (2001) 603–632.
[2] Z.T. Zhu, J.L. Musfeldt, H.J. Koo, M.H. Whangbo, Z.S. Teweldemedhin, M. Greenblatt, Chem. Matter. 14 (2002) 2607–2615.
[3] V. Bondarenko, J.W. Brill, J. Dumas, C. Schlenker, Solid State Commun. 129 (2004) 211–215.
[4] M. Greenblatt, Int. J. Mod. Phys. B 7 (1993) 3937–3971.
[5] A. Martínez-de la Cruz, F.H. Guillén Garza, U. Ortiz Méndez, L.M. Torres-Martínez, Adv. Tech. Mat. Mat. Process. J. (ATM) 7 (2005) 131–134, ISSN 1440-0731.
[6] A. Martínez-de la Cruz, L.M. Torres-Martínez, U. Ortiz Méndez, Adv. Tech. Mat. Mat. Process. J. (ATM) 7 (2005) 167–170, ISSN 1440-0731.
[7] A. Martínez-de la Cruz, F.E. Longoria Rodríguez, J. Ibarra Rodríguez, Solid State Ionics 176 (2005) 2625–2630.
[8] P. Roussel, Ph. Labbé, D. Groult, Acta Cryst. B56 (2000) 377–391.
[9] R. Herrera Sánchez, L. Treviño, A.F. Fuentes, A. Martínez-de la Cruz, L.M. Torres, J. Solid State Electrochem. 4 (2000) 210–215.
[10] S. Patoux, C. Masquelier, Chem. Mater. 14 (2002) 2334–2341.
[11] E. Baudrin, S. Laruelle, S. Denis, M. Touboul, J.M. Tarascon, Solid State Ionics 123 (1999) 139–153.
[12] Y. Chabre, Prog. Solid State Chem. 23 (1995) 1–130.
[13] F.E. Longoria Rodríguez, Ph. Thesis, Universidad Autónoma de Nuevo León (2006).
[14] A. Martínez-de la Cruz, F. García-Alvarado, E. Morán, M.A. Alario-Franco, L.M. Torres-Martínez, J. Mater. Chem. 5 (3) (1995) 513–516.
[15] E. Wang, M. Greenblatt, J. Solid State Chem. 68 (1987) 38–44.